Seismic Through Simulation with Integrated Time-Lapse Workflow*

Travis Ramsay[1], Jesse Lomask[1], and Jimmy Ting[2]

Search and Discovery Article #41938 (2016)**
Posted November 14, 2016

*Adapted from extended abstract based on oral presentation given at AAPG/SEG International Conference & Exhibition, Cancun, Mexico, September 6-9, 2016

[1]Halliburton, Houston, TX (Travis.Ramsay@halliburton.com)
[2]CGG, Houston, TX

Abstract

This work illustrates a high-fidelity seismic to simulation workflow employed in a mature field. To demonstrate the fidelity of the employed method, a dual quantitative cross-validation through time-lapse inversion workflow incorporating petro-elastic modeling (PEM) in time as well as depth is used to enhance the interpretive capability of seismic reservoir properties for engineers. *A priori* planning of reservoir and simulation spatial grid scales is performed to help minimize the impact of resampling and upscaling on the time-dependent analysis of seismic and simulation reservoir properties. The accuracy of the solution is validated by comparing the relative difference between concurrent seismic and flow simulation results.

The methods employed in the execution of this study attempt to reconcile seismic and simulation in depth- and time-driven time-lapse workflows to exploit bypassed pay and examine infill drilling potential. The early cross-domain consideration of scale and accurate velocity modeling help minimize upscaling ambiguities and resampling artifacts typically introduced in classical workflows.

Introduction

The execution of four-dimensional (4D) reservoir monitoring studies has classically been performed in anomaly interpretation of mature fields; however, it has become highly valuable as a tool used extensively in reservoir management for bypassed pay analysis, defining pressure compartmentalization and fluid flow characteristics of faults, monitoring fluid contacts, dynamic rock-type classification, and seismic-based history matching (Lumley and Behrens, 1998; Emerick et al., 2007; Ramsay and Yarus, 2015). These studies have demonstrated added value by incorporating fit-for-purpose modeling strategies to increase recovery from the asset, but they can also be leveraged to provide low-cost 4D feasibility assessment to evaluate the costs and technical risks associated with executing 4D projects, which is crucial in the current low-price oil environment.

A high-fidelity seismic to simulation workflow is executed for a mature field case study spanning seismic interpretation to reservoir simulation for bypassed pay identification with requisite infill drilling. Associated with the study is an examination of cross-domain technological collaboration, which highlights risk and uncertainty minimization by maintaining consistency between the subsurface model and historical production. This consistency is achieved by relating the simulation results to the seismic, and vice versa, leading to more accurate business decisions.

A significant component of the 4D workflow is its integration with dynamic reservoir data (Johnston, 2013), which enables an important link to production to help enable subsurface and surface consistency through a unified model. The evaluation of consistency between the seismic inversion and the reservoir simulation model is achieved through a PEM. Classically, PEM has been performed as a post-process to the execution of the numerical flow model; however, contemporaneous efforts have focused on the concurrent execution of the PEM as a part of a systematic and simultaneous process within the reservoir simulator. This allows one-way coupling of the flow response to the PEM so that dynamic elastic properties are computed as a direct result of the evolution of the pressure profile and fluid phase distribution computed in the reservoir simulator.

Theory and Methodology

Four horizons through the zone of interest were interpreted. Then three wells with density, p-wave, and s-wave logs were tied to the seismic using synthetic analysis. During this process, wavelets were extracted and used in subsequent time-lapse seismic inversion step. From the inversion process, elastic properties (p-velocity, s-velocity, and density) and engineering properties (volume of clay, effective porosity, and permeability) were generated as input for reservoir modeling and flow simulation.

It is possible to reconcile the numerical flow response of production to the geophysical description through the application of a PEM. In the utilized model, the elastic response of the subsurface is simultaneously coupled with the numerical flow simulation to describe pressure- and saturation-induced changes in the reservoir. The commercial reservoir simulator incorporates the defined PEM implicitly as a post-process to the subsurface Darcy flow solution. Two PEM methods are executed for the purpose of the modeling exercise: the Batzle and Wang (1992) (BW) method and a simulator-driven method. The former is prescribed following BW and is based on an empirical formulation combining thermodynamic relationships with trends relating pressure and solid-fluid composition. The latter is explicitly defined according to existing fluid properties, characterized by pressure-volume-temperature (PVT) relations, in the reservoir simulation and the corresponding relation to modeled elastic properties through Gassmann's equation.

The newly defined simulator-driven PEM is based on determining the saturated bulk modulus by the computed compressibility from the simulator (K_{fluid}, K_{φ}) in addition to static mineral rock matrix moduli, which are incorporated from the existing static model ($K_{mineral}$). The dry rock bulk modulus, which represents the porous media drained of fluids, is computed according to Eq. 1 (Emerick et al., 2007; Mavko et al., 2009):

$$\frac{1}{K_{dry}} = \frac{1}{K_{mineral}} + \frac{\varphi}{K_{\varphi}} \; where \; \frac{1}{K_{\varphi}} = \frac{1}{v_{pore}} \frac{\partial v_{pore}}{\partial \sigma} \qquad (1)$$

Where $K_{mineral}$ is the bulk modulus of the intrinsic mineral material, φ represents the time-dependent effective porosity fraction (adjusted by net-to-gross and the pore volume multiplier computed from rock compaction), K_{φ} is the pore space stiffness, and σ is the stress induced by the pore pressure. The term $\frac{1}{K_{\varphi}}$ is computed in the reservoir simulator as $C_{\varphi} = \frac{1}{K_{\varphi}} = \frac{1}{v_{pore}} \frac{\partial v_{pore}}{\partial \sigma}$, where C_{φ} is the compressibility of the pore space. Considering the pore space as being modified by fluids, the superposition of the inverse mineral bulk modulus and the inverse modulus of the pore space modified by fluids leads to the determination of the bulk modulus of the saturated pore space ($K_{saturated}$) in Eq. 2 (Emerick et al., 2007; Mavko et al., 2009):

$$\frac{1}{K_{saturated}} = \frac{1}{K_{mineral}} + \frac{\varphi}{K_{\varphi} + \frac{K_{mineral} K_{fluid}}{K_{mineral} - K_{fluid}}} \quad (2)$$

Here, K_{fluid} is the bulk modulus of the pore fluid. K_{fluid} can be determined by Wood's equations (Eq. 3) (Emerick et al., 2007; Mavko et al., 2009), which describes the saturation-weighted inverse bulk modulus through harmonic averaging as

$$\frac{1}{K_{fluid}} = \frac{S_{water}}{K_{water}} + \frac{S_{oil}}{K_{oil}} + \frac{S_{gas}}{K_{gas}}; \; for \; S_{water} + S_{oil} + S_{gas} = 1 \quad (3)$$

Here, $\frac{1}{K_{fluid}}$ is the fluid compressibility C_{fluid}, which is also determined by the reservoir simulator. The saturated rock density is computed following the previous description of modeled dry rock matrix density.

The results of this workflow demonstrate a fit-for-purpose model resolution across seismic interpretation, simultaneous inversion, petrophysical property modeling, and reservoir simulation performed in collaboration across a multidisciplinary process to illustrate bypassed pay analysis.

Discussion

The field considered in this case study is located offshore West Africa (Figure 1), following Marquez et al. (2013). The primary target is a Miocene turbidite channel system with no major faults. The reservoir simulation model comprises three producers, of which one is a vertical well and the remaining two are sidetracks. A water injection scenario is investigated from a proximal well to evaluate the potential for increased recovery in the intermediate zone. The comprehensive model domain contains 84 x 64 x 163 grid-blocks possessing a nominal dimension of 13 x 26 x 1 meters, and the grid geometry is 1092 x 1664 x 163 meters. The PVT used in the simulator is treated as black-oil with a medium-grade oil characterized by 37° API.

The zone of interest is located between 1900 and 2200 m depth (approximately in the middle of the vertical orientation of Figure 1). Particular attention is focused in Figure 1 on the zones near the injector at 2100 m depth and approximately half-way between the injector and producer at 2150 m depth that show no changes in impedance after 3 years of production.

The rock-fluid description of the reservoir simulation model was characterized according to a binary sand-shale lithological description. Corey-type relative permeability curves were assigned directly to the lithological description based on the assumption that the hydraulic rock types were adequately described by lithology, following the electrofacies description of Perez et al. (2003) and Rushing et al. (2008) but in a sand-prone reservoir. Larger capillary number flows, indicative of increased flow velocity and oil displacement capability, were associated with the sand while lower capillary number flows, indicative of decreased flow velocity and displacement capability, described the shale component of the model. The elastic property descriptions are analogous to local considerations (Sone and Zoback, 2013; Habib et al., 2016). Scaling of the elastic properties to match the inversion result was minimally performed. After one simulated year of production, the water front progressed approximately 550 meters, the shale sequences remain saturated with oil, as anticipated, and much of the sand has been swept by the injected water; however zones began to accumulate in the sand where characterized pay remains behind the water front. These zones form potential bypassed pay, which are simultaneously identified in the inversion of the monitor seismic.

After 3 years of simulated production, as observed in Figure 2, the simulator-driven PEM is sensitive to the evolution of the saturation profile and fluid type distribution, while the BW PEM is sensitive to the response of the pressure profile. This is evident after a comparison with Figure 3, where the saturation and pressure profiles after 3 years of simulation are illustrated. The potential bypass pay zones commensurate with the 4D inversion in Figure 1 are identified as lower-unmodified impedance attributes along the well section. The interwell cross-section in Figure 4 highlights subtle changes in the simulator-driven dynamic p-impedance resulting from the change in saturation, while the sensitivity of the BW-derived dynamic p-impedance in the sand and shale rock types is shown to occur across varied depths.

Potential bypass pay is also considered to exist near the producer sufficiently after breakthrough. Figure 5 shows an isolated section surrounding the producer and similarly demonstrates lower-unmodified zones of p-impedance. In order to emphasize the domain agnostic capability of the current workflow, the dynamic p-impedance computed by the reservoir simulator is converted from the depth to the two-way time domain, as illustrated in Figure 5. This particular characteristic of the workflow enhances cross-discipline collaboration between the reservoir simulation engineer and the geophysicist by enabling a singular subsurface representation, irrespective of the domain in which the analysis is conducted.

An analogous observation that minor changes in PEM derived p-impedance resulting from the simulator-driven PEM compared to the BW PEM is maintained in Figure 4 and Figure 5. Further analysis of the simulation results in Figure 6, which show impedance computed in a single gridblock by both PEM methods, reveals that PEM-derived impedances demonstrate time-dependent variation that would best be understood with higher rates of seismic acquisition with requisite inversion. In the absence of more frequent inversion results for validation, a fluid dynamic characterization would suggest low sweep efficiency is manifested as the absence of piston-like displacement of in-place oil by water, which resulted in partially swept and unswept zones. Concurrent to the benefit of time-lapse inversion is the ability to conduct the 4D study incorporating a reservoir simulator that enables the relation of dynamic response with acquired seismic.

Conclusion

It is observed that there is some variation between the results analyzed in the time and depth. The variation in the results is typically caused by the types of inversion methods, PEM methods, and vertical and spatial resampling used. In this study, however, the effect of vertical and spatial resampling is diminished by the omission of petrophysical property model upscaling from the integrated workflows. The omission of upscaling by *a priori* spatial grid sampling considerations reduced overall inaccuracies from being introduced into the comparative quantitative analysis. As a corollary, the trade-off with the increased gridblock resolution is reservoir simulator performance. The processes used by the overall workflow are mostly agnostic to time- or depth-domain driven collaboration; therefore, they can easily be fully or partially incorporated into any existing workflow with simplicity to enable rapid and accurate reservoir decision making. The final results show cross-domain bypassed pay analysis through efficient, streamlined interpretation and simulation.

Acknowledgements

The authors acknowledge CGG for providing the dataset as well as the management of Halliburton and CGG for granting permission to complete this case study. Additionally, the authors thank Felix Segovia with Halliburton and Santi Randazzo with CGG for their assistance with completing this case study, and Dominic Camilleri from the Nexus reservoir simulation team for his assistance in implementing the PEM feature as a part of the simulator.

References Cited

Batzle, M., and Z. Wang, 1992, Seismic properties of pore fluids: Geophysics, v. 57/11, p. 1396-1408.

Emerick, A., R. Jesus de Moraes, and J. Rodrigues, 2007, Calculating seismic attributes within a reservoir flow simulator: SPE No. 107001-MS, presented at the Latin American & Caribbean Petroleum Engineering Conference, April 15-18.

Habib, M., S. Charles, Y. Guangqing, and M. Danlami, 2016, An inversion of reservoir properties based on concurrent modeling approach: The case of a West African reservoir: Journal of Petroleum Exploration and Production Technology, p. 1-12.

Johnston, D., 2013, Practical applications of time-lapse seismic data: SEG Distinguished Instructor Series, No. 16.

Lumley, D., and R. Behrens, 1998, Practical issues of 4D seismic reservoir monitoring: What an engineer needs to know: SPE Reservoir Evaluation and Engineering, v. 1/6, p. 528-538.

Marquez, D., D. Saussus, R. Bornard, and J. Jimenez, 2013, Incorporating rock physics into geostatistical seismic inversion – case study: Presented at the 75th EAGE Conference & Exhibition incorporating SPE EUROPEC, June 10-13.

Mavko, G., T. Mukerji, and J. Dvorkin, 2009, The Rock Physics Handbook, Tools for Seismic Analysis of Porous Media, second edition, New York: Cambridge University Press.

Perez, H., A. Datta-Gupta, and S. Mishra, 2003, The role of electrofacies, lithofacies, and hydraulic flow units in permeability predictions from well logs: A comparative analysis using classification trees: SPE No. 84301, presented at the SPE Annual Technical Conference and Exhibition, October 5-8.

Ramsay, T., and J. Yarus, 2015, Petrofacies determination in unconventional reservoirs driven by a simulation-to-seismic process: SPE No. 174295-MS, presented at SPE EUROPEC, June 1-4.

Rushing, J.A., K.E. Newsham, and T.A. Blasingame, 2008, Rock typing – keys to understanding productivity in tight gas sands: SPE No. 114161-MS, presented at the SPE Unconventional Reservoirs Conference, February 10-12.

Sone, H., and M. Zoback, 2013, Mechanical properties of shale-gas reservoir rocks – Part 1: Static and dynamic elastic properties and anisotropy: Geophysics, v. 78/5, D381-D392.

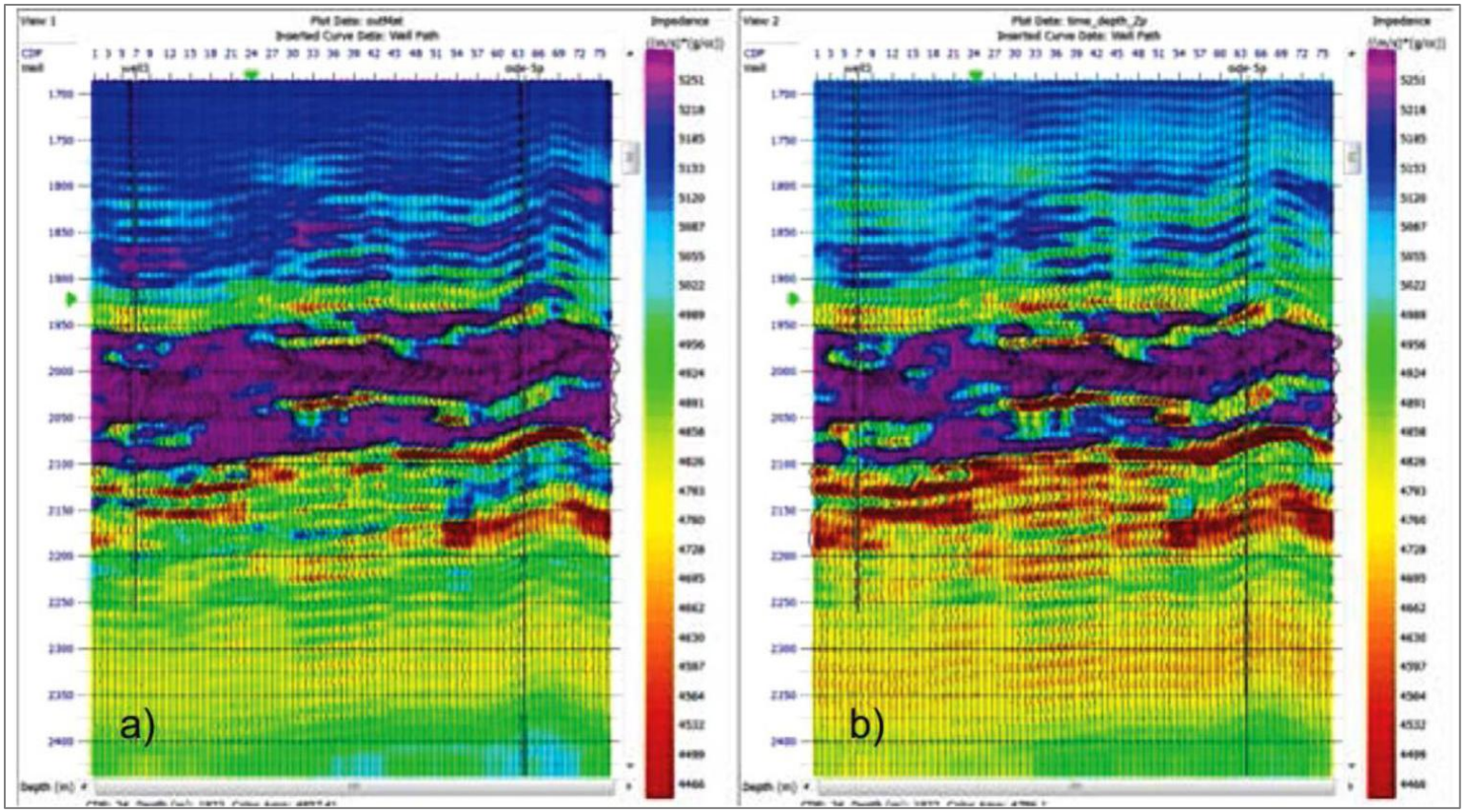

Figure 1. 4D seismic inversion of the West African field. Illustrated are (a) the inversion of the monitor survey after 3 years of production, and (b) the base survey inversion. The time-lapse effect could be observed by the overall increase in p-impedance on the monitor survey.

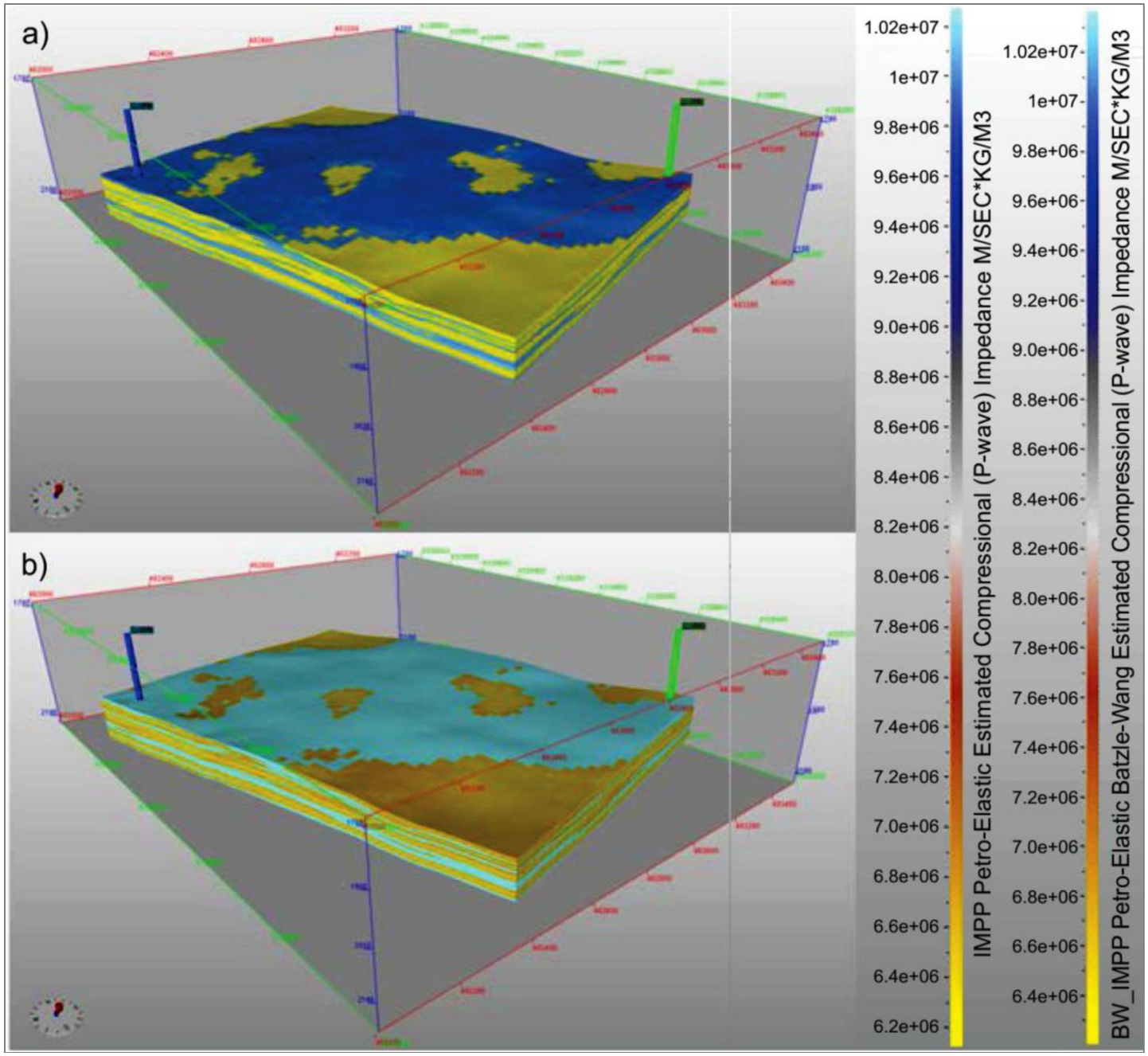

Figure 2. Three-dimensional (3D) visualization of simulator-driven (a) PEM, and (b) BW. PEM results after 3 years for an intermediate layer of the model.

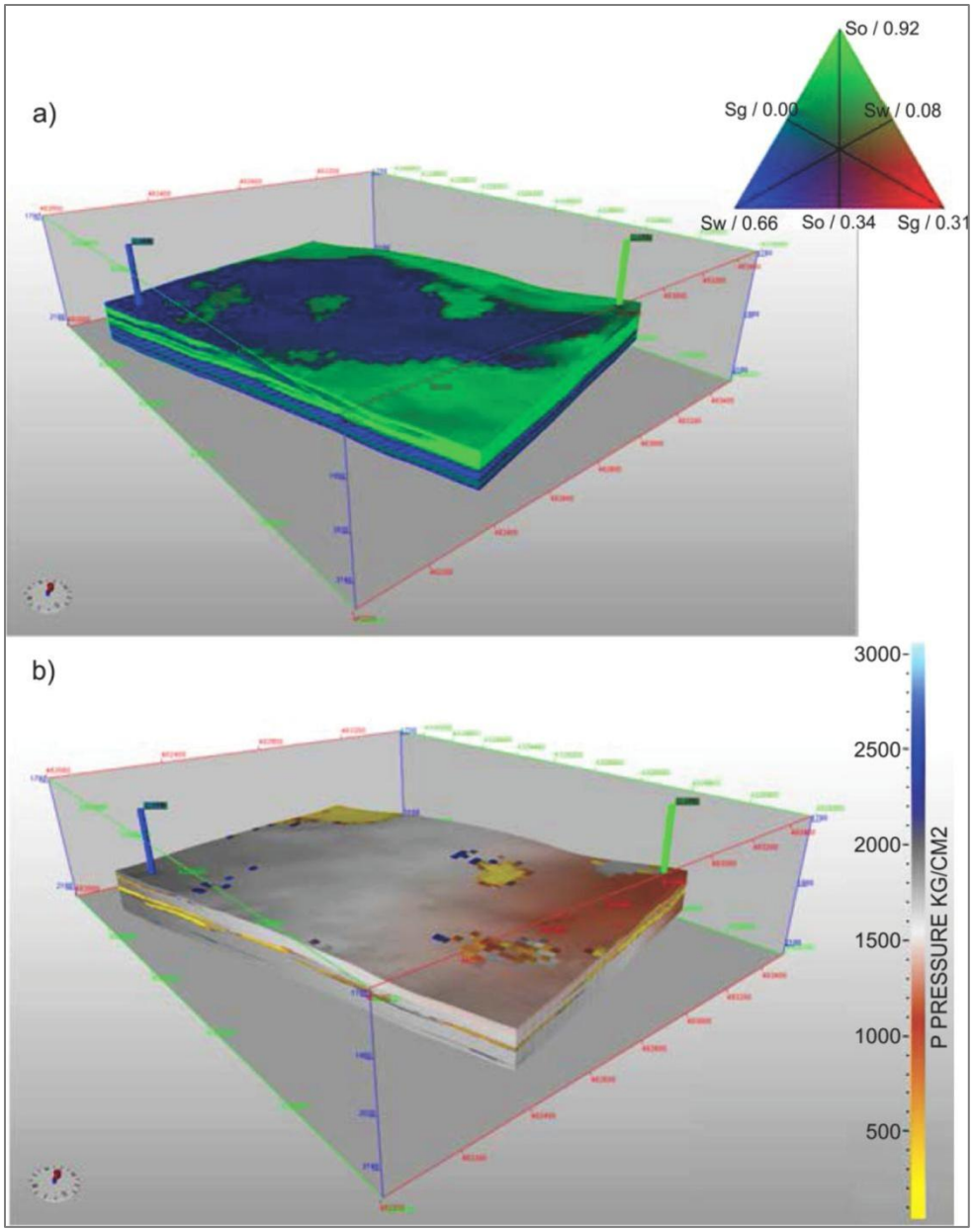

Figure 3. 3D visualization of (a) saturation profile, and (b) dynamic pressure profile after 3 years.

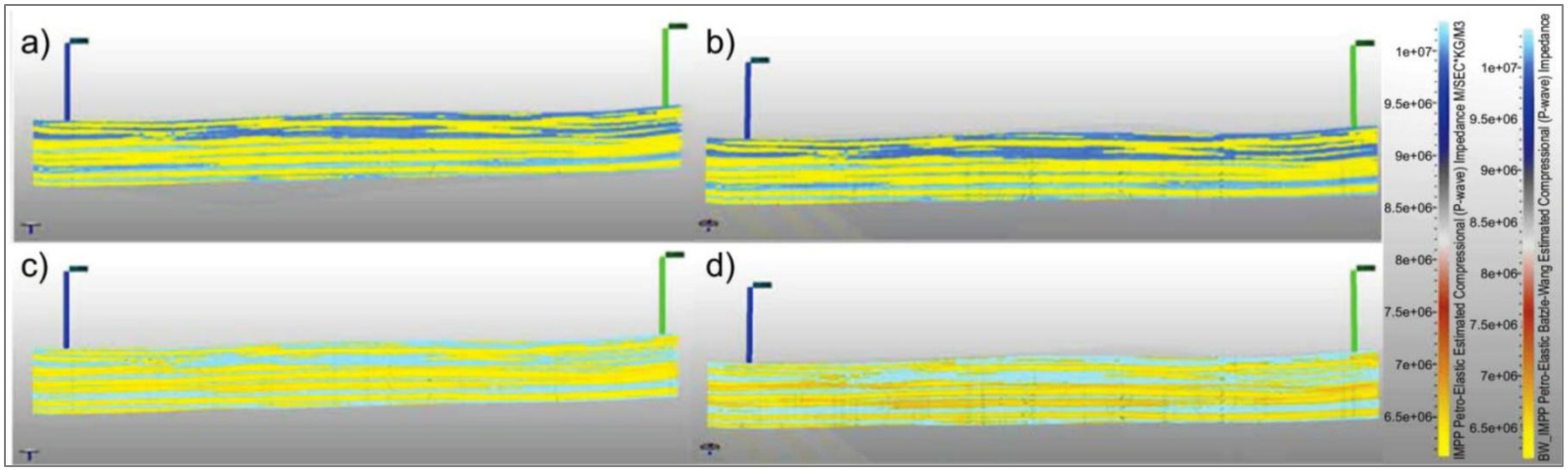

Figure 4. PEM-derived p-impedance slice: (a) simulator-driven method at time = 0 years, (b) simulator-driven method at time = 3 years, (c) BW method at time = 0 years, and (d) BW method at time = 3 years, PEM results.

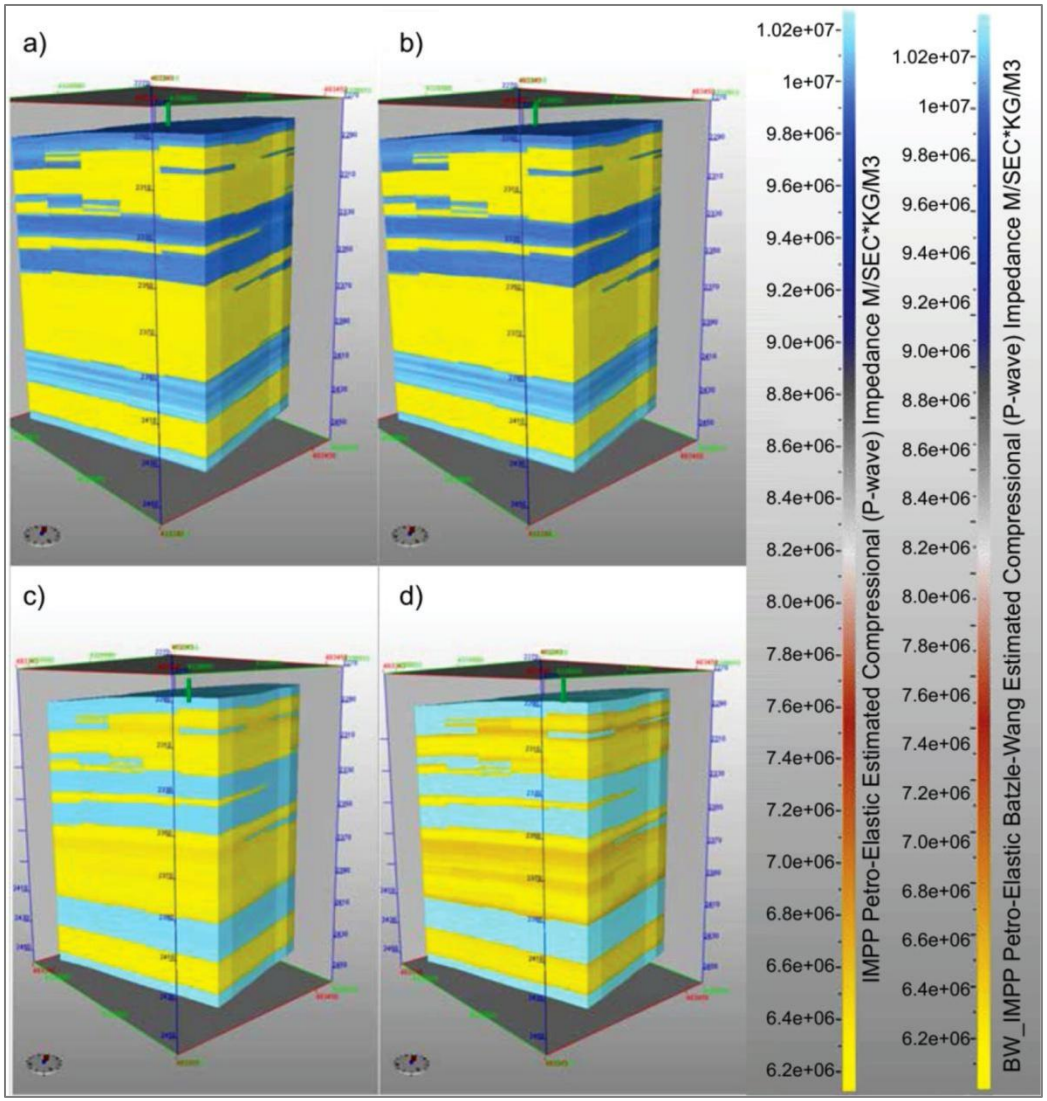

Figure 5. PEM-derived dynamic p-impedance near producer in two-way time domain: (a) simulator-driven method at time = 0 years, (b) simulator-driven method at time = 3 years, (c) BW method at time = 0 years, and (d) BW method at time 3 years.

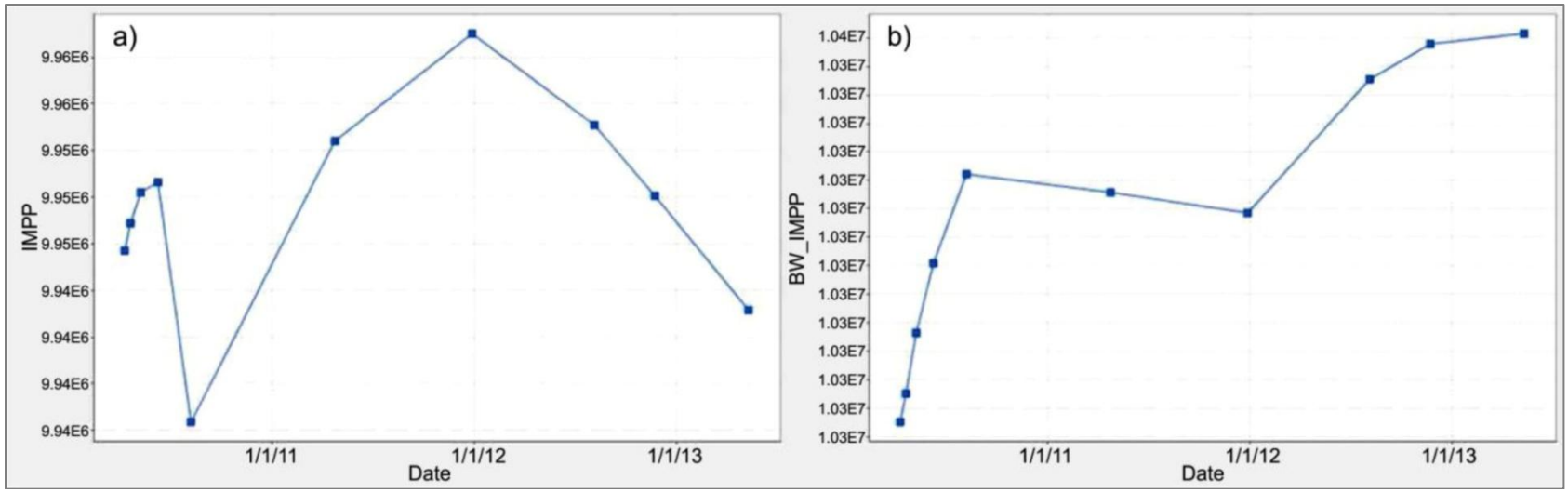

Figure 6. Illustration of (a) simulator-driven PEM p-impedance, and (b) BW PEM p-impedance for a single gridblock situated between the injector and producer on Layer 30 of the model.